JAAS

Cite this: *J. Anal. At. Spectrom.*, 2011, **26**, 2189

www.rsc.org/jaas

PAPER

Measurement of carbon solubility in magnesium alloys using GD-OES†

Hai-Lin Chen,[a] Nan Li,[a] Andre Klostermeier[b] and Rainer Schmid-Fetzer*[a]

Received 14th April 2011, Accepted 6th July 2011
DOI: 10.1039/c1ja10128e

It is shown that the quality of the internal atmosphere in glow discharge lamps has a crucial effect on the carbon measurement. Recipes, including atmosphere quality checking, atmosphere purification by burning dummy samples, prolonged preburning time and frequent drift corrections, are developed to reliably measure carbon content in trace amounts. The carbon solubilities in magnesium, which are in the order of magnitude of tens of ppm, are consequently measured for the first time. A new route of sample preparation of Mg–C alloys is presented to avoid heterogeneity and contamination. The method for evaluating the crater volume was also advanced.

Introduction

Magnesium alloys have the potential to serve as functional as well as biomaterials.[1,2] This investigation was triggered by the measurement of the carbon solubility in magnesium and its alloys, which has never been measured but is believed to be negligible since the carbon composition has not been documented in any specification of magnesium alloys.

Glow discharge optical emission spectrometry (GD-OES) with the conventional direct current (dc) Grimm-type atomization/excitation source has been extensively used for bulk analysis, depth profile analysis and trace analysis of conductive materials.[3,4] It appears to be a promising method for measuring trace amounts of carbon in magnesium, but significant difficulties may exist in preparing homogeneous and contamination-free Mg–C samples and in trace carbon analysis. Many factors may contribute to the background of carbon in a GD-OES measurement, including the electronic and spectral backgrounds, the contamination in the sample during the sample preparation, the residual gas in the lamp, and the leakage of the air, *etc.* Kim *et al.*[5] determined the carbon background, excluding the electronic and spectral backgrounds, to be about 24 ± 10 ppm, under conditions of 800 V and 8 torr Ar in a LECO GDOES750A instrument.

Furthermore, suitable Mg–C calibration standards are unavailable and a multi-matrix calibration is needed in GD-OES measurements. The calibration between intensity and concentration considering the sputtering rates (SR) of multi-matrix materials can be performed by the model of Weiss:[6]

$$I_i^m = R_i \cdot q^m \cdot c_i^m + b_i + \sum_{j \neq i} a_{ij} \cdot I_j^m \quad (1)$$

In this general function, the intensity of element i in the material m, I_i^m, is expressed in three terms. The first term is due to the element i sputtered from the material m, where c_i^m is the concentration of element i in material m, q^m is the sputtering rate of material m, and R_i is the emission yield, which is assumed to be independent of the material matrix despite the fact that it is not.[7] The second term is the matrix-independent background due to electrical signal noise and depends on instruments and experimental conditions. The third term is the matrix-dependent background due to the intensity contributions from other elements. The latter could be negligible, if the spectral line for an element to be measured had been carefully selected, so eqn (1) reduces to[8]

$$I_i^m = R_i \cdot q^m \cdot c_i^m + b_i \quad (2)$$

Sputter rates depend on the properties of the material, experimental conditions and instruments. For materials containing two or more components, a preferential sputtering commonly exists, so sputtering rate in the initial stage is larger than that in the steady-state sputtering.[9] As another consequence of preferential sputtering, the material surface is deficient in readily sputtered elements but rich in slowly sputtered elements. When a steady-state sputtering is attained, the surface composition should remain constant which is different from the bulk composition, but the sputtered materials per unit time should have the same composition as the bulk materials. Thus the measured intensities during steady-state sputtering could reflect the concentration of the material. From the conservation of the mass at equilibrium,[10] the equilibrium sputtering rate is given by

[a]*Robert-Koch Strasse, 42, D-38678 Clausthal-Zellerfeld, Germany. E-mail: schmid-fetzer@tu-clausthal.de; Fax: +49 5323 72 3120; Tel: +49 5323 722150*
[b]*LECO Instrumente GmbH, Marie-Bernays-Ring 31, D-41199 Moenchengladbach, Germany*

† Electronic supplementary information (ESI) available: Sample numbers, designations, and nominal compositions of the Mg- and Fe-matrix calibration standards used in this work. See DOI: 10.1039/c1ja10128e

$$\frac{1}{q^m} = \frac{1}{100} \cdot \sum_i \frac{c_i^m}{q_i^m} \quad (3)$$

where q_i^m is the sputtering rate of the element (i) in the matrix (m), which would be a fictitious quantity and not identical to the sputter rate of the pure element (q_i) due to the effect of the bounding energy of the atom in the matrix if $i \neq m$. This equation can be employed to evaluate sputtering rates with constant values of q_i^m for each component, but generally should be restricted to a single matrix, or be employed in a narrow composition range. However, Ren *et al.*[11,12] found that the element sputter rates could be approximated to those of pure elements in many systems.

The sputter rate (normally given in the unit of μg s^{-1}) can be experimentally determined by measuring the weight loss or the volume of the sputtered crater. The volumetric method is generally thought to be superior to the gravimetric method, because of the significant difference between the total sample mass and the sputtered mass and the redeposition of the sample material on the crater edge.[8]

In this work we present a new method for preparing Mg–C alloys, conduct sputter rates measurements of the involved alloys, and perform a GD-OES analysis of carbon, so as to determine the carbon solubilites in magnesium.

Experimental procedure

Mg–C alloy preparation

Raw materials were pure magnesium pieces (99.99 wt. %, ChemPur, Germany) and graphite crucibles (99.9995%, SGL group, Germany). The crucibles have an inner diameter of 30 mm, a wall thickness of 5 mm, and a height of 60 mm. In this method, magnesium melt directly reacts with the graphite crucible to form saturated liquid solutions at the experimental temperature (from 700 to 900 °C, with intervals of 50 degrees) and then the liquid alloys will be frozen by quenching.

The furnace was first heated up to a setting temperature. About 20 g Mg materials were loaded in a graphite crucible and the crucible was then put into the vertical furnace chamber made of a corundum tube. Ar gas (4N) was led in by a corundum pipe, which was firstly descended into the crucible just above the Mg materials, to expel air from the crucible and the furnace chamber. After several minutes, the Ar pipe was elevated above the crucible, a steel lid was loaded on the crucible, and the furnace was covered, as shown in Fig. 1. The experimental setup was then held at that temperature in the flowing argon atmosphere for a time varying from 0.5 h to 2 h. After the heat treatment, the furnace cover and the Ar pipe were first removed. After further removing the crucible lid, the crucible was immediately taken out and quickly quenched with about one third of its height dipped in cold water. The time interval between removing the crucible lid and dipping the crucible in the water is about 10 s or less.

The obtained cylindrical ingots have a diameter of 30 mm and a height of about 15 mm. The upper surfaces are rather irregular and are usually covered by dark carbon and grey magnesium oxide, but the thickness is no more than 1.5 mm. The bottom surface and lateral surface, which are in contact with the graphite crucible, however, are quite smooth and clean. The upper layers were removed by grinding and the measurements began with the bottom surfaces.

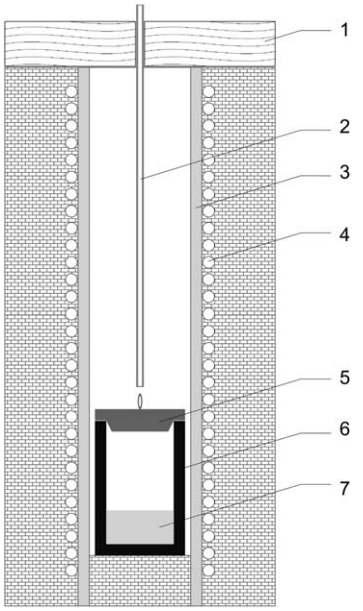

Fig. 1 Experimental setup for melting Mg–C alloys: (1)-furnace cover, (2)-argon gas pipe, (3)-corundum chamber, (4)-heating element, (5)-crucible lid, (6)-graphite crucible, (7)-Mg materials.

GD-OES experiments

The GD-OES measurements were conducted on GDS850A instrument (LECO) using an anode of 4 mm, with a constant applied voltage (700 V) and a constant applied current (20 mA). The instrument was always kept on for the duration in which all the measurements in this work were conducted, but the Ar supply may be switched off if there are no measurements for more than one week.

Before starting measurements on a new day, a standard procedure suggested by LECO[13] was followed, including warming up the glow discharge lamp (GDL), collecting the PMT offset, profiling the instrument, and drift corrections. Afterwards, measurements of non-gaseous elements can be started. For carbon, however, the quality of the internal atmosphere in GDL was usually not good enough for measurements at that point. As explained in more detail in the section "Recipes for carbon measurement", a certified reference material (CRM) with a low carbon content was used to check the atmosphere quality, and hours of burns using dummy samples were necessary to improve the internal atmosphere quality, especially if the instrument had not been used and the argon supply had been turned off for some days.

Without Mg-matrix standards for carbon calibration, a multi-matrix calibration method had to be employed and some Fe-matrix CRMs were selected. In order to bridge the calibration between Fe-matrix standards and Mg-matrix samples, the calibration lines should be corrected by the sputtering rates. To corroborate the validity of the sputtering rate-corrected calibration, some Mg reference materials (RMs) were also used as calibration standards. All the standards are listed in the ESI†

with numbers, designations and nominal compositions. The Fe-matrix and Mg-matrix standards were carefully selected such that both groups of standards provide a compatible distribution of the composition of some elements, such as Mn and Si. As a result, calibration lines of Mn and Si could be created using both groups of standards and by considering the sputter rates of individual standards, and the consistency could be checked.

All samples were ground by SiC sandpapers from P400 to P800 grit or P1200 grit. Standards or samples whose carbon contents needed to be measured were additionally ground with P1200 Alumina grinding belt, cleaned ultrasonically in water, and blow-dried to remove possible carbon contamination. Other samples were ultrasonically cleaned in ethanol. In order to check the homogeneity of the carbon distribution in the as-cast Mg–C samples, measurements were first performed on their bottom surfaces after being slightly ground, and then the samples were further ground to remove a certain layer of material so that different sections could be examined.

It is well known that a preburn is needed for an intensity measurement to attain a steady-state sputtering, as well as to remove the possible contaminations on the sample surfaces. In order to set an appropriate preburn time, several testing measurements on Mg and Fe alloys were conducted. It was found that a 90 s preburning appeared enough for most analytes (elements), while 200 s was necessary for carbon measurement, under the presently applied voltage and current. The burning time was set at 10s and typically three burns were successively conducted at each crater, with the averaged value taken as one data point.

Crater profiling

In this work, sputtering rates of samples and standards were determined volumetrically, *i.e.* by measuring the volume of the craters burned in the GDS850A instrument under the same conditions of applied voltage and applied current as the intensity measurements. For this purpose, depths of craters were profiled with a mechanical profilometer (KLA-Tencor Alpha Step 500, USA). Craters burned on both Mg-alloys and Fe-alloys have the diameter of almost exactly 4 mm according to optical microscopic examinations. This is because of the perfect geometry of the Grimm-type lamp, which constricts the discharge physically to the inside of the anode tube.[8] The line scanning distance was set to be 5 mm to cross the whole crater. A scanning step of 2 μm was chosen to achieve a good resolution for volume evaluation. Baseline calibration was performed for each profile by extrapolating the baseline from the flat segments corresponding to the sample surface.

Strictly speaking, sputtering rates of materials should be measured during steady-state sputtering, in which the intensities are measured. The initial sputter rate of a material (before a steady-state sputtering is attained) may be much higher than the steady-state sputter rate, because of the preferential sputtering. Practically, however, a sputter rate measurement cannot be conducted only in a steady state. One can only increase the total sputtering time, to increase the impact of the steady-state sputtering, thus reducing the effect of the initial stage on the sputter rate determination. In this work, different burning times (100 s, 190 s and/or 300 s) were tried and these experiments were conducted separately from the intensity measurements.

Combustion analysis

The results from our GD-OES measurements show that magnesium can dissolve carbon only in tens of ppm. As a supplementary method, a Carbon/Sulfur Analyzer (CS 230, LECO) was utilized to tentatively measure the carbon solubility in four magnesium samples, 750C1hA, 800C2h, 850C1hA and 900C1hB.‡ Three to five measurements were conducted for each sample, and the sample amount varied from 0.5 g up 1.5 g.

Results and discussion

Volume evaluation of craters

Fig. 2 presents the profile of one crater in the stainless steel sample 9Co5Mo18Ni after 300 s burn under the conditions of 700 V and 20 mA, which shows a very good resolution for volume evaluation. The crater shape is typical for all the samples and standards involved in this work. The edge of the crater noticeably sticks out above the sample surface, *i.e.* the depth of zero, which indicates a significant redeposition of the sputtered materials. In fact, the sputtered materials could also redeposit on the inner surface of the crater, so a dynamical equilibrium would be established during the steady state and result in an "effective" sputtering rate, as pointed out by Bengtson.[8]

The measured crater depth profile can be fitted piecewise by arbitrarily selected functions. The fitted profile was then used to evaluate the volume of the crater by integration since the crater can be regarded as roughly rotation-symmetric. In fact, each half of the profile is enough to reproduce the crater by rotating 360° along a vertical axis at the center. Since the profile may be more or less asymmetric, both the two halves of the profile should be

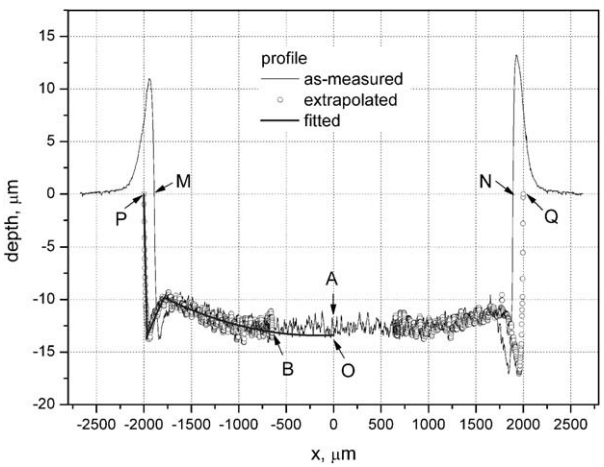

Fig. 2 Depth profile of a crater on the stainless steel sample 9Co5Mo18Ni after 300 s burn. Thin line: as-measured profile; circles: the extrapolated data; and thick line: the fitting curve.

‡ The name "900C1hB" indicates that the sample was heated at 900 °C for 1 h, and more than one sample was prepared under the same conditions, so this is the sample B.

utilized such that the averaged value could be a better approximation to the volume of the real crater. This method was recently presented by Martin *et al.*[14] and it is much more reliable than the standard approximation that treats craters as regular cylinders. However, a normal 2D profilometer may be incapable of ensuring that the scanning line passes through the center of the crater. Fig. 3a presents the 3-D simulation of the crater whose profile had been presented in Fig. 2, and Fig. 3b is its projection on the XOY plane. Since the scanning line may not exactly pass through the crater center, the distance from M to N (*i.e.* the length of the segment M′N′) is less than the diameter of the crater, and the depth at the midpoint A less than that at the center (O). One can also observe a similar problem in the work of Martin *et al.*[14] Unfortunately, they ignored the problem, which may cause an error of 10% or more.

Therefore, this work presented a method to reasonably extrapolate a profile, PQ, which is through the crater center, from the as-measured profile MN, as seen in Fig. 2 and Fig. 3. The extrapolated profile, and not the as-measured one, should be used for evaluating the volume of the crater. The extrapolation was conducted based on the assumption that all the points on the same circle have the same depth. This assumption will be violated if the crater is asymmetric, but it has been implied in the integration method which treats the crater as rotation-symmetric. Moreover, since both halves of the profile are independently used to simulate the crater, the effect of asymmetry has already been taken into account. Fig. 3b is the projection of the 3-D crater in Fig. 3a onto the XOY plane, and the projection of each point will be indicated with a prime (′) except for the center O since it coincides with its projection. The crater center was taken as the origin (0,0,0). Now an arbitrary point C on the measured profile should be extrapolated to D (x,y,z). The two points have the same z coordinate since they were assumed to have the same depth. Since the extrapolated profile is located on the XOZ plane, the y coordinate is zero. Since both points are located in the same circle, the distance between D′ and O, *i.e.* the magnitude of the x coordinate, is equal to the length of OC′.

$$|x| = \overline{OD'} = \overline{OC'} \tag{4}$$

$$\overline{OC'}^2 = \overline{A'C'}^2 + \overline{A'O}^2 \tag{5}$$

$$\overline{A'O}^2 = \overline{M'O}^2 - \overline{A'M'}^2 \tag{6}$$

where the length of A′M′ and A′C′ can be read from the as-measured profile, and M′O is the true radius of the crater. It is worth noting that the midpoint A is not to be extrapolated to the origin O but point B. In fact, no data can be used to directly build up the part BO, including the origin O. However, once the part PB was well determined and fitted, the remaining part BO can be reasonably extrapolated, as seen in Fig. 2. Due to its features, the profile BP can be divided into three segments to be separately fitted with arbitrarily selected functions.

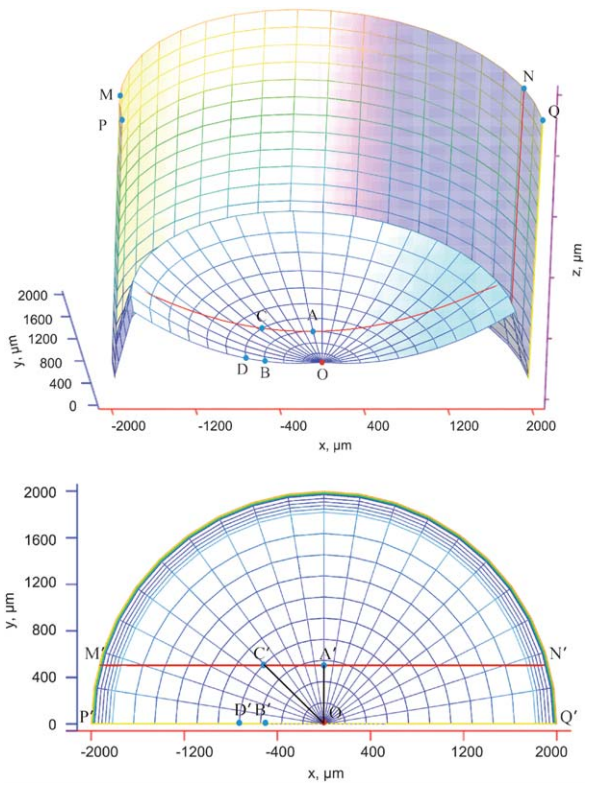

Fig. 3 Simulation of the profile in Fig. 2: (a) the 3-D crater and (b) its projection on the XOY plane.

Sputtering rates

The sputtering rates were calculated in μg s^{-1} derived from the measured volumes, the burning time, and the material densities. The densities of all the steels were calculated using the measured

Table 1 Measured sputter rates of irons/steels and Mg alloys

Number	Sample name[a]	SR, μg s^{-1}	±σ, μg s^{-1}	RSR
1	100Fe	3.29	0.11	1.00
2	1Al1Ni	3.32		1.01[b]
	19Cr1Mn10N			
3	i	3.34		1.01[b]
4	9Cr	3.35	0.06	1.02
5	1Mn	3.35		1.02[b]
6	12Cr	3.36	0.15	1.02
7	5Al22Cr	3.45		1.05[b]
8	17Co29Ni	4.06	0.08	1.24
9	9Co5Mo18Ni	4.11	0.12	1.25
10	AXZ921	3.33	0.15	1.01
11	AZ91D	3.45	0.08	1.05
12	AZ91S	3.81	0.02	1.16
13	AMS501	3.27	0.15	0.99
14	AM60B	3.76	0.15	1.14
15	AM50D	3.74	0.09	1.14
16	AM50S	3.89	0.05	1.18
17	AS21	3.59	0.09	1.09
18	AZ51	3.87	0.04	1.18
19	AZ31	4.28	0.14	1.30
20	Ce3	4.75	0.13	1.44
21	Mg–C	3.62	0.07	1.10

[a] Samples no. 1–20 are designated by the main alloying elements and their approximate weight percents. For example, 1Al1Ni is a steel, containing about 1 wt.% Al and 1 wt.% Ni; AXZ921 is a Mg alloy, where A indicates Al, X Ca, and Z Zn, and their weight percents are about 9, 2 and 1, respectively. More details are given in the ESI.† [b] Sputter rates of four steels are evaluated by sputter rate fitting.

volumes and weights. The densities of all magnesium alloys were calculated from the weighted sum of the volumes of all components. Table 1 presents the sputter rates of both Fe-matrix alloys (no. 1–9) and Mg-matrix alloys (no. 10–21) measured in this work. Most data were measured volumetrically, but for the four Fe-alloys (1Mn, 1Al1Ni, 5Al22Cr, 19Cr1Mn10Ni), their sputter rates were estimated in a sputter rate fitting by taking into account the calibration lines of the selected analytes. The sputter rates were also plotted in Fig. 4, with relative values, RSR, to the low alloy steel 100Fe, in which its alloying elements are less than 0.3% in total. The error bar was defined as the magnitude of the sample standard deviation.

The sputter rates of both Fe- and Mg-matrix alloys investigated in this work are comparable in magnitude in $\mu g\ s^{-1}$, and the relative values vary only between 0.95 and 1.35 except for the magnesium alloy Ce3. In particular, the Mg–C alloys cast in this work have a relative sputter rate of only 1.1. Because of the density ratio (4.53/1) of Fe/Mg, the sputtered volume or depth is about four times higher for Mg- compared to Fe-alloys under the same conditions.

For materials of the same matrix, if the composition does not change much or for a certain group of materials, the difference in their sputter rates was often neglected practically. For example, one might assume that all irons and steels have the same sputter rate, or that "cast irons" have the same sputter rate but differ from that of "stainless steels". This simple treatment is because data of sputter rates are often rare. In fact, the deviation of the sputter rates among "stainless steels" may be as "significant" as that between stainless steels and cast irons, based on the present results. Sputter rates significantly depend on the compositions. The low-alloy steel (100Fe) has the lowest sputter rate among the Fe alloys involved in this work and the value would possibly be very close to pure iron and other low alloy steels, simply because these alloys have low alloying element content. Two stainless steels, 9Cr and 12Cr, which contain Cr up to 9.1% and 12.4%, respectively, have sputter rates only slightly higher than the low-alloy steel, because Cr has a close sputter rate to pure Fe.[15] The stainless steel 9Co5Mo18Ni and the special alloy 17Co29Ni have sputter rates 25% higher than 100Fe. This is because of the large total content of Co and Ni, together with Mo. It was reported that Co, Ni and Mo have sputter rates of 1.8, 1.5 and 1.3 relative to Fe,[15] respectively. A simple estimation of the sputter rates was conducted by using eqn (3) and taking into account the main alloying elements and the matrix element Fe, and gave values of 1.13 and 1.21 for 9Co5Mo18Ni and 17Co29Ni, respectively. The calculated values were somewhat lower than the experimental results, but adequately indicated the noticeable increment of the sputter rate. The differences may be partly caused by the approximation of q_i^m as the sputter rates of pure elements.

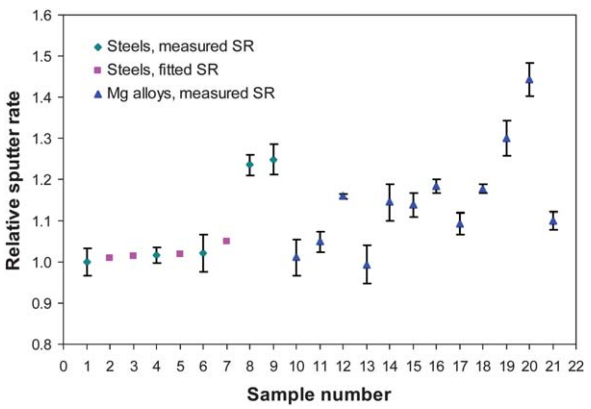

Fig. 4 Sputter rates of Fe- and Mg-matrix alloys relative to the low-alloy steel 100Fe (no. 1). Most data were measured volumetrically and error bars were defined as the standard deviations. Sputter rates of the four Fe-alloys (no. 2, 3, 5 and 7) were estimated in a sputter rate fitting.

The sputter rates of the other four Fe-alloys (1Mn, 1Al1Ni, 5Al22Cr, 19Cr1Mn10Ni) were estimated in a sputter rate fitting by taking into account the calibration lines of the selected analytes of all the Fe-alloys. During that fitting the sputter rates of the Fe-alloys no. 1, 4, 6, 8 and 9 were fixed by the experimental values. The sputter rates of 1Mn and 1Al1Ni are almost 1.0 since their total alloying content is less than 4%. 5Al22Cr contains Al at 5.3% and 22.3% Cr. Al is believed to decrease the sputter rate of the steel.[15] Therefore, an estimated sputter rate of 1.05 appears reasonable. The estimated value for 19Cr1Mn10Ni is only about 1.0, which agrees well with the value of 1.03, calculated by taking into account only Fe, Cr and Ni.

Multi-matrix calibration

Since there are no commercial CRMs containing magnesium and carbon available, a multi-matrix calibration taking into account the sputter rate correction had to been utilized. In this work, a number of CRMs or RMs of irons/steels and Mg alloys were carefully selected, based on the consideration that not only does the carbon content in irons/steels vary over a considerable range to establish a reliable calibration line, but also both irons/steels and Mg alloys share good variations in the Mn and Si contents. The latter provides an opportunity to check the reliability of the sputter rate correction. If the sputter rates were reliably determined, consistent calibration lines for Mn and Si could be established based on the results from both groups of materials.

In fact, since the relative sputter rates of most Mg- and Fe-based standards are in a narrow range from 1.0 to 1.3, which is almost comparable with the difference among the "stainless steels", the calibration line of carbon determined from Fe-alloys could be directly employed for Mg–C alloys even without taking into account the sputter rate correction in a crude simplification.

It was found that the matrix-dependent background can be neglected and eqn (2) is good enough to calibrate Mn and Si. Since the sputter rates were preferably given in a relative value, the following equation suggested by Payling *et al.*,[10] which is intrinsically the same as eqn (2), was used:

$$q_{rel}^m \cdot c_i^m = a_i \cdot I_i^m - b_i \qquad (7)$$

The two coefficients, a_i and b_i, are to be evaluated during regression, and should have positive values. Fig. 5 shows the present calibrations based on both irons/steels and Mg alloys with a preburn of 90 s, and the data points from standards of both matrices appear to be quite consistent. Fig. 6 presents the calibration lines for carbon determined from the irons/steels with preburn times of 90 s and 200 s, which indicate that the as-measured carbon intensities with a preburn of 90 s contain higher background than those with a preburn of 200 s. The latter

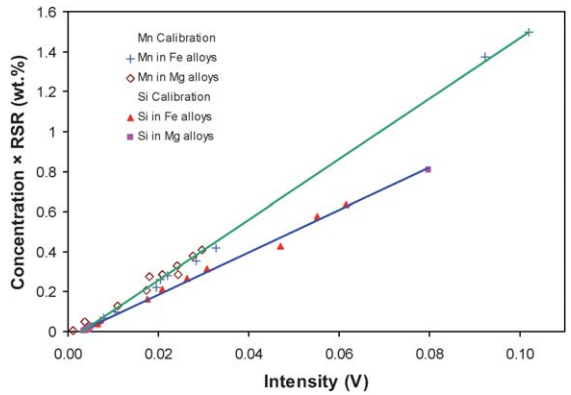

Fig. 5 Calibration lines for Mn(I) 403.4 nm and Si(I) 288.0 nm determined from both Fe and Mg alloys, taking into account the sputter rates.

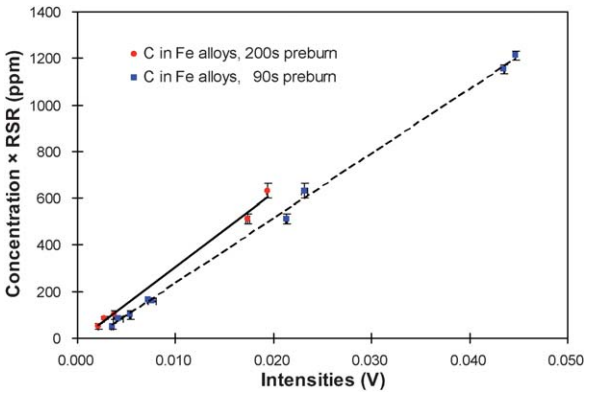

Fig. 6 Calibration line for C(I) 165.0 nm determined from irons/steels, taking into account the sputter rates.

calibration line can be fitted with coefficients of $a_i = 31\ 799$ and $b_i = 13.157$, and was finally employed to determine the carbon concentration in the Mg–C alloys. The value of b_i corresponds to a total background of 12 ppm for carbon in the measurement of Mg–C alloys if taking into account their relative sputter rate of 1.1. It is noticeably lower than the value of 24 ± 10 ppm determined by Kim *et al.*,[5] in which the electronic and spectral contributions were even excluded. This is a significant improvement achieved in this work, which is probably due to the following recipes made for carbon measurements.

Recipes for carbon measurements

A reliable measurement of carbon is far more difficult than for other non-gaseous elements, especially in trace amounts. Many factors affect the measurement of carbon, such as the surface contamination of the samples due to grinding with SiC sandpapers and rinsing in organic solvent, the impurities in Ar, the leakage of the air between the sample and the O-ring, and the atmosphere contamination in the GDL. The surface contamination of the samples could be reduced by grinding with alumina sandpapers and not rinsing samples in organic solvents. The impurities in Ar itself could be neglected since the C impurity in ultra high purity (5N) Ar should be less than 1 ppm. However, the Ar atmosphere in the GDL can be easily polluted.

It was experimentally confirmed that the contamination in the internal atmosphere of the GDL may be significant. This was done by regularly measuring the raw carbon intensity of a drift standard 9Co5Mo18Ni having a nominal carbon concentration of 40 ppm, from the beginning of a day's measurements. As shown in Fig. 7, the carbon intensities, which have been normalized with the last value, are unsteady and decrease dramatically in the first 2 h, and gradually tend towards stability after 3 h. In contrast, the quality of the atmosphere may have a negligible effect on the measurement of non-gaseous elements. As an example, the observed raw Ni intensity (normalized with the last value) in this drift standard was also plotted in Fig. 7. It was steady from the very beginning. It should be noted that the initial quality of the internal atmosphere in the GDL depends on the condition of the equipment; for example, if experiments have been run in recent days and the argon has been kept on. Sometimes, it could take longer to attain a steady state. As a consequence, a standard procedure of pre-measurements including warming-up GDL, collecting the PMT offset, profiling the instrument, and drift correction may not be sufficient for measurements of carbon. Generally, the internal atmosphere of the GDL is not of good quality at the beginning of one day's measurements, especially if no measurements have been conducted and/or the Ar supply had been cut off for some days. Therefore, the procedure in Fig. 7 should be employed as a standard procedure for carbon measurement. Before real samples are measured, the drift standard of carbon should be regularly measured (about every half hour) until the intensities become steady or reach a predetermined low value. During the interval of measuring the drift standard, a dummy sample (steel reference material SUS CFe1/5, with a nominal carbon content of 40 ppm) is measured. The real samples can be measured only after the internal atmosphere reaches a better quality. It is recommended to continue to run the drift standard regularly, because the atmosphere quality is still slowly improving. Even though the observed carbon intensities generally tend to become steadier and lower, chaotic fluctuation is also present. It may not be sufficient to run a drift correction only at the beginning, as is

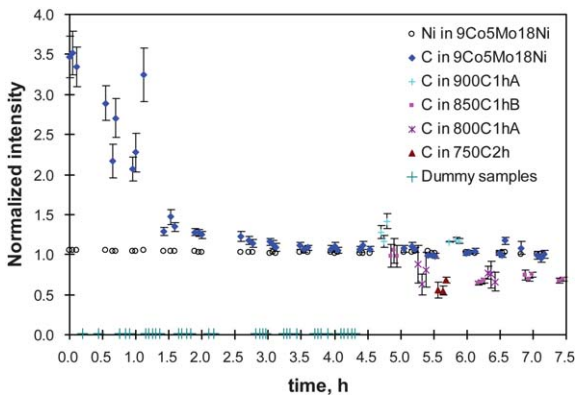

Fig. 7 A typical procedure for measuring carbon: the drift standard (9Co5Mo18Ni) was measured three times every half an hour, a dummy sample was burned at each interval during the first 4.5 h, and samples were alternately measured after the steady state was attained. All the raw intensities of C and Ni were normalized with the relevant value of 9Co5Mo18Ni in the last measurement. The intensities of the dummy sample were not plotted for better readability.

the procedure for non-gaseous elements. If possible, the Ar supply should be left on after a day's measurements to maintain a better quality of the internal atmosphere for another day.

It is well known that a preburn is needed to achieve a steady-state sputtering, as well as to eliminate possible contamination on the sample surfaces. Because of the internal atmosphere contamination, the preburning is much more important to the carbon measurement and a much longer preburning time is needed. A preburning of 90 s is generally suitable for non-gaseous elements, but much too short for carbon, as evidently shown in Fig. 8, as well as in Fig. 6. In this work, a 200 s preburn was finally employed for carbon measurement. Such a long preburning greatly reduced the effect of the internal atmosphere on the intensity measurements, so the as-measured intensities included less background and were less scattered. Besides, the time for the atmosphere purification by using dummy samples was shortened. In other words, the measurement became less sensitive to the quality of the internal atmosphere.

Carbon concentration

The samples prepared at 700 °C and 750 °C did not yield reliable results in either GD-OES or combustion measurements. It is mainly because the samples did not melt well at low temperatures. Cracks and pores present in these samples frequently result in bad electronic conductivity in the GD-OES measurement. Table 2 presents only the results measured at 800 °C, 850 °C and 900 °C by GD-OES. For each sample, the data obtained by using a preburn of 90 s or 200 s are comparable, but a longer preburn obviously results in a higher accuracy and the data resulting from a preburn of 200 s have standard deviations less than 4 ppm. It is worth noting that additional to the statistically derived standard deviations, an extra error of 5 ppm due to the drift correction should be considered for each piece of data in order to estimate the real experimental uncertainties. Combustion measurements yielded values of 79.3 ± 17.3, 53.6 ± 7.4 and 72.6 ± 5.0 ppm for the samples 900C1hB, 850C1hA and 800C2h, respectively. These data appear less reliable, since the value at 800 °C is larger than that at 850 °C by 20 ppm. However, these data are also in tens of ppm, which may provide qualitative support to the data from GD-OES. It is recommended to only consider the data measured by GD-OES with a preburn of 200 s, which has been marked in bold font in Table 2, for evaluating the carbon solubility in magnesium. The solubility may be reasonably extrapolated to a wider temperature range in a future Calphad[16] modeling of the Mg–C system, by incorporating other phase equilibria data and thermodynamic data available for this system in the literature.

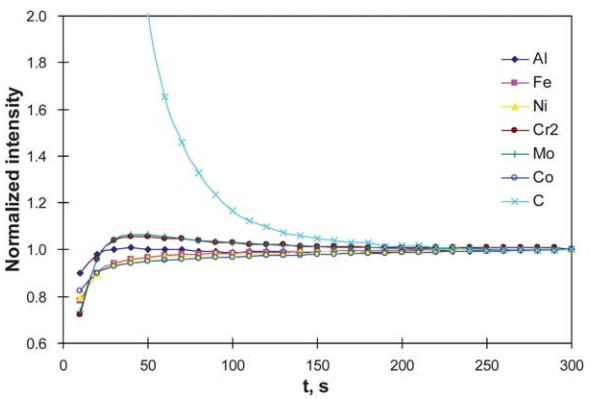

Fig. 8 Measured intensities in 9Co5Mo18Ni for the first 300 s burning. The intensity of each element was normalized with the last value at 300 s.

Table 2 Measured carbon contents in as-cast Mg–C alloys by GD-OES

Sample	C content, ppm	Preburn time[a]
900C1hA	69 ± 8	90 s
	64.8 ± 2.0	**200 s**
900C1hB	52 ± 8	90 s
850C1hA	40 ± 7	90 s
850C1hB	33 ± 3	90 s
	32.0 ± 1.5	**200 s**
850C1hC	31 ± 7	90 s
	28.3 ± 3.3	**200 s**
800C1hA	31 ± 6	90 s
	20.1 ± 3.2	**200 s**
800C1hB	18 ± 5	90 s
	18.0 ± 1.6	**200 s**
800C2h	20 ± 7	90 s
800C0.5h	—	90 s
	14.1 ± 2.1	**200 s**

[a] The samples 900C1hB, 850C1hA and 800C2h were measured by GD-OES only with a preburn of 90 s and were then consumed by combustion measurements.

Conclusion

The atmosphere quality in glow discharge lamps has a critical effect on the measurement of carbon. As in recipes developed in this work, the atmosphere quality should be checked with a known drift standard and can be improved by burning dummy samples before conducting real measurements, and the pre-burning time of each measurement should be appropriately determined based on experiments. The carbon solubility in liquid Mg was measured for the first time in this work from 800 °C to 900 °C. A new route of sample preparation and a new method of evaluating crater volume were also presented.

Acknowledgements

The authors acknowledge the financial support by the German Research Foundation (DFG) in the Priority Programme "SPP 1473" under grant no. Schm 588/37.

Notes and references

1 R.-G. Guan, T. Zhao, L.-L. Wang and T. Cui, *Adv. Mater. Res.*, 2009, **79–82**, 1443.
2 T. Narushima, *Metals for Biomedical Devices*, 2010, 355.
3 C. Xhoffer and H. Dillen, *Berg- und Huettenmaennische Monatshefte*, 2007, **152**, 18.
4 R. Heyner, S. Maennel and G. Marx, *LaborPraxis*, 1995, **19**, 28.
5 Y. S. Kim, V. Hoffmann and D. Schiel, *Bull. Korean. Chem. Soc.*, 2002, **23**, 525.
6 Z. Weiss, *J. Anal. At. Spectrom.*, 1995, **10**, 891.
7 Z. Weiss, *Spectrochim. Acta, Part B*, 1993, **48**, 1247.
8 A. Bengtson, *Spectrochim. Acta, Part B*, 1994, **49**, 411.
9 Y. Homma, H. Takenaka, F. Toujou, A. Takano, S. Hayashi and R. Shimizu, *Surf. Interface Anal.*, 2003, **35**, 544.
10 R. Payling, M. Aeberhard, J. Michler, C. Authier, P. Chapon, T. Nelis and L. Pitchford, *Surf. Interface Anal.*, 2003, **35**, 334.

11 J. Ren, G. Zhang, Z. Wang, G. Liu and S. Liu, *Acta Metall. Sin.*, 1992, **5**, 462.
12 J. Ren, G. Zhang, Z. Wang and J. Zhao, *J. Mater. Sci. Technol.*, 1995, **11**, 295.
13 *GDS850 Atomic Emission Spectrometer, Version 4*, 2003, LECO Corporation.
14 A. Martin, A. Martinez, R. Pereiro, N. Bordel and A. Sanz-Medel, *Spectrochim. Acta, Part B*, 2007, **62**, 1263.
15 T. Neilis, R. Payling, *Glow discharge optical emission spectroscopy: a practical guide*, 2003, pp.90.
16 L. Kaufman, *CALPHAD: Comput. Coupling Phase Diagrams Thermochem.*, 2001, **25**, 141.

